

## Guided ultrasonic wave beam skew in silicon wafers

Marco Pizzolato, Bernard Masserey, Jean-Luc Robyr, and Paul Fromme

Citation: [AIP Conference Proceedings](#) **1949**, 090005 (2018); doi: 10.1063/1.5031568

View online: <https://doi.org/10.1063/1.5031568>

View Table of Contents: <http://aip.scitation.org/toc/apc/1949/1>

Published by the [American Institute of Physics](#)

---

### Articles you may be interested in

[Methodologies for validating ray-based forward model using finite element method in ultrasonic array data simulation](#)

[AIP Conference Proceedings](#) **1949**, 080002 (2018); 10.1063/1.5031559

[A non-collinear mixing technique to measure the acoustic nonlinearity parameter of adhesive bond](#)

[AIP Conference Proceedings](#) **1949**, 070005 (2018); 10.1063/1.5031557

[Sensitivity images for multi-view ultrasonic array inspection](#)

[AIP Conference Proceedings](#) **1949**, 080001 (2018); 10.1063/1.5031558

[Defect imaging in composite structures](#)

[AIP Conference Proceedings](#) **1949**, 130004 (2018); 10.1063/1.5031599

---

# Guided Ultrasonic Wave Beam Skew in Silicon Wafers

Marco Pizzolato<sup>1</sup>, Bernard Masserey<sup>1</sup>, Jean-Luc Robyr<sup>1</sup>, Paul Fromme<sup>2a</sup>

<sup>1</sup>Department of Mechanical Engineering, University of Applied Sciences, Fribourg, Switzerland

<sup>2</sup>Department of Mechanical Engineering, University College London, WC1E 7JE, UK

*[pfromme@ucl.ac.uk](mailto:pfromme@ucl.ac.uk)*

**Abstract.** In the photovoltaic industry, monocrystalline silicon wafers are employed for solar cells with high conversion efficiency. Micro-cracks induced by the cutting process in the thin wafers can lead to brittle wafer fracture. Guided ultrasonic waves would offer an efficient methodology for the in-process non-destructive testing of wafers to assess micro-crack density. The material anisotropy of the monocrystalline silicon leads to variations of the guided wave characteristics, depending on the propagation direction relative to the crystal orientation. Selective guided ultrasonic wave excitation was achieved using a contact piezoelectric transducer with custom-made wedges for the  $A_0$  and  $S_0$  Lamb wave modes and a transducer holder to achieve controlled contact pressure and orientation. The out-of-plane component of the guided wave propagation was measured using a non-contact laser interferometer. The phase slowness (velocity) of the two fundamental Lamb wave modes was measured experimentally for varying propagation directions relative to the crystal orientation and found to match theoretical predictions. Significant wave beam skew was observed experimentally, especially for the  $S_0$  mode, and investigated from 3D finite element simulations. Good agreement was found with the theoretical predictions based on nominal material properties of the silicon wafer. The important contribution of guided wave beam skewing effects for the non-destructive testing of silicon wafers was demonstrated.

**Keywords:** Elastic Anisotropy, Lamb Wave Modes, NDE, Skew Angle, Phase Slowness

**PACS:** 43.20.Mv, 43.35.Zc, 43.35.Cg

## INTRODUCTION

Solar photovoltaic electricity generation is an important renewable energy source. In order to improve its competitiveness, higher conversion efficiency and lower production costs of the solar panels are required. This relies on the improvement of the production processes to obtain thinner silicon wafers, which are very fragile. The minimum wafer thickness is in practice determined by the breakage rates due to small cracks induced during the wafer sawing and final assembly [1]. Several non-destructive testing methods have been considered for the in-line detection of cracks and structural defects in silicon wafers during the manufacturing process, including thermography, impact testing, ultrasonics, and photo-luminescence imaging [2, 3]. Guided ultrasonic waves can propagate over long distances [4, 5] and have been proposed for the monitoring of silicon wafers during the production process. Damage detection in metallic structures was achieved using high frequency guided waves [6, 7]. Non-contact laser excitation and measurement of the fundamental Lamb wave modes was used for crack detection in silicon wafers [8]. Monocrystalline and polycrystalline silicon wafers for solar cells were tested using non-contact air-coupled transducers to detect cracks [9].

The energy focusing of longitudinal and transverse ultrasonic waves in anisotropic materials can be theoretically predicted [10]. The velocity dependency on the wave propagation direction relative to the crystallographic orientation in thick silicon plates was measured and compared to theory [11]. The anisotropic material properties can be obtained from an inversion of experimental results [12]. The zero group velocity of guided waves in silicon wafers was measured using a line laser source, showing amplitude and cut-off frequency variation for directions with different stiffness [13]. Guided wave propagation in silicon wafers was measured to study the variation in arrival time and amplitude with propagation direction [14]. Similarities exist to the guided wave propagation in composite plates [15], where the energy concentration [16] and mode focusing was studied [17]. The influence of the anisotropic material properties on the angular dependency of the wave propagation characteristics in thin monocrystalline silicon wafers was investigated [18]. The fundamental guided wave modes ( $A_0$  and  $S_0$ ) were excited using a wedge transducer and measured using a non-contact laser interferometer. Experimental results were compared to Finite Element (FE) simulations.

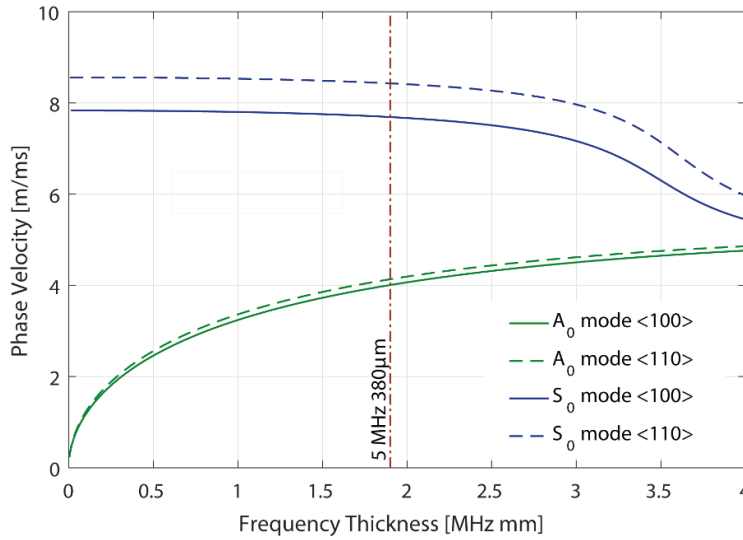


**FIGURE 1.** Phase velocity dispersion curves of fundamental  $A_0$  and  $S_0$  modes for monocrystalline silicon wafer. Dispersion curves computed for principal crystallographic directions  $\langle 100 \rangle$  (solid) and  $\langle 110 \rangle$  (dashed). Vertical line (dash-dotted) represents frequency thickness product for 5 MHz excitation in 380  $\mu\text{m}$  thick wafer.

### GUIDED WAVE PROPAGATION IN ANISOTROPIC MEDIA

The anisotropic material properties of silicon result in a dependency of the guided ultrasonic wave characteristics on the propagation direction relative to the crystal orientation. The group and phase velocities of the  $A_0$  and  $S_0$  Lamb modes were calculated using Disperse [19] for a 380  $\mu\text{m}$  thick silicon wafer (stiffness constants for  $\langle 100 \rangle$  orientation, corresponding to azimuth angle  $\varphi = 0^\circ$  ( $C_{11} = 165.70$  GPa,  $C_{12} = 63.90$  GPa,  $C_{44} = 79.56$  GPa)). The phase velocities of the  $A_0$  and  $S_0$  modes for the  $\langle 100 \rangle$  and  $\langle 110 \rangle$  crystal orientations are shown in Fig. 1. For the  $\langle 110 \rangle$  direction, which has the highest stiffness, higher phase velocities will be observed. The frequency thickness product of the 5 MHz excitation frequency and 380  $\mu\text{m}$  wafer thickness, which corresponds to our experimental conditions, is indicated in Fig. 1. At this frequency thickness product, the phase velocity of the  $A_0$  mode varies by approximately 3% between the two crystal orientations, while a larger direction dependent difference of 10% can be observed for the  $S_0$  mode. The theoretically predicted phase slowness (inverse of phase velocity) as a function of the propagation direction is shown as the solid line in Fig. 2. It exhibits the  $45^\circ$  symmetry of the silicon material anisotropy, with lower phase slowness (higher phase velocity) at  $45^\circ$  than at  $0^\circ$  and  $90^\circ$ .

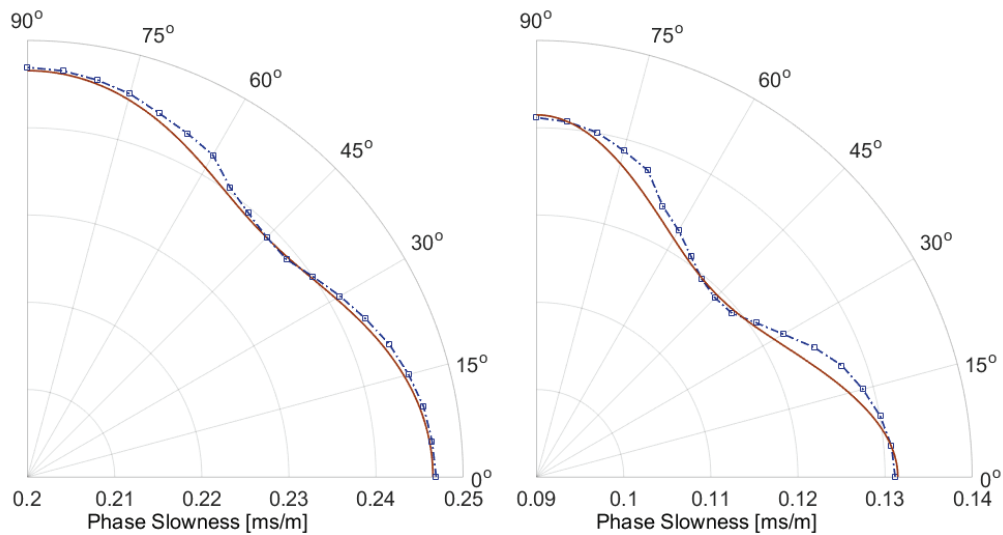


**FIGURE 2.** Phase slowness curves for (left)  $A_0$  mode and (right)  $S_0$  mode in 380  $\mu\text{m}$  thick silicon wafer, 5 MHz frequency;  $\langle 100 \rangle$  orientation corresponds to azimuth angle  $\varphi = 0^\circ$ ; solid: theoretical calculation; dots: experimental measurement.

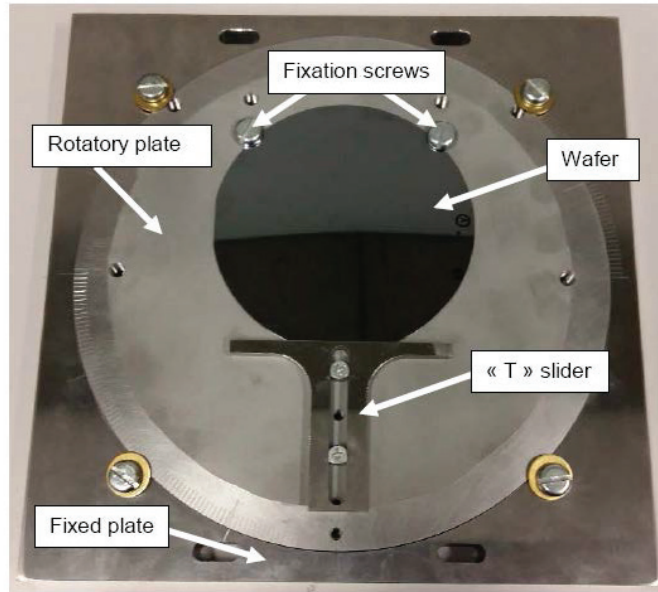


**FIGURE 3.** Wafer holder with silicon wafer disc, fixated by T-slider and screws, allowing angular rotation with  $0.5^\circ$  step size.

### EXPERIMENTAL SETUP

Experimental measurements were conducted in boron doped single crystal silicon wafers with  $\langle 100 \rangle$  crystallographic orientation, 100 mm diameter and  $380 \mu\text{m}$  nominal thickness. The silicon wafers were held by a custom-made holder (Fig. 3) to reduce the risk of wafer breakage and to allow precise angular orientation of the wafer with an accuracy of approximately  $0.5^\circ$ . Guided wave excitation was achieved using custom-made nylon wedges with a commercial piezoelectric transducer. Wedges were manufactured with respectively  $41^\circ$  ( $A_0$  mode) and  $19^\circ$  incident angles ( $S_0$  mode) to selectively excite each of the first fundamental Lamb modes. Figure 4 shows the second holder developed and manufactured to control the contact pressure and orientation of the angle beam transducer relative to the silicon wafer.

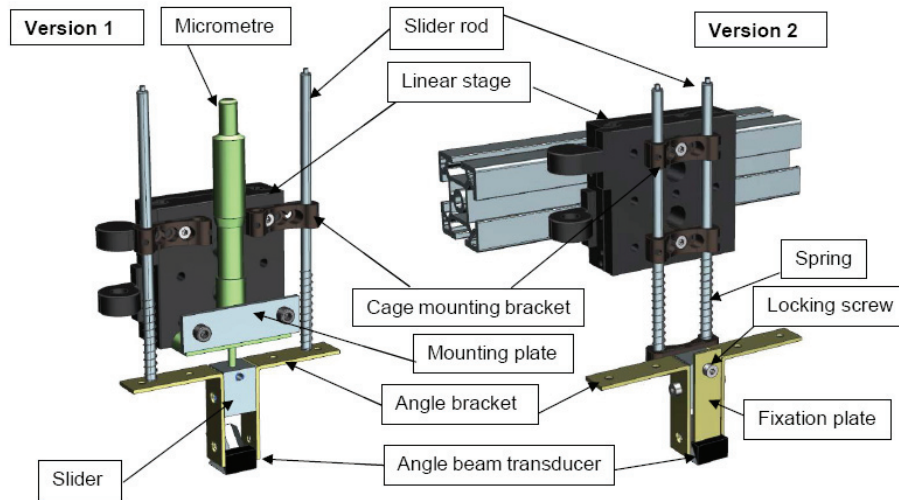


**FIGURE 4.** Two versions of the developed angle beam transducer holders that control the contact pressure and orientation relative to the silicon wafer.

The narrowband excitation signal had a center frequency of 5 MHz and consisted of 12 cycles in a Hanning window. The signal was generated using an arbitrary function generator, amplified using a power amplifier, and applied to the angle beam transducer. The velocity of the out-of-plane displacement was measured using a non-contact laser interferometer, moved parallel to the wafer on a scanning rig. The voltage signal was frequency filtered (bandpass: 2-7 MHz), averaged (50 averages) and transferred from the oscilloscope to the PC using Labview.

## PHASE VELOCITY

The phase velocity was measured in the far field (40 mm from wedge) with steps of 0.2 mm over a distance of 10 mm. This was done for 5° angular steps over a 90° range, rotating the wafer from the <100> crystal direction (azimuth angle  $\varphi = 0^\circ$ ) via the <110> direction ( $\varphi = 45^\circ$ ) to the <010> direction ( $\varphi = 90^\circ$ ), with the same material properties as the <100> direction. For each measurement point, a time gate based on the group velocity was applied around the wave pulse of interest and Fast Fourier Transform (FFT) was used to obtain the phase value. Phase jumps were removed and the phase velocity was obtained from a linear fit of the phase as function of distance data. The comparison to the theoretically calculated phase slowness curves as function of the propagating angle is shown in Fig. 2. Good agreement was found with the theoretically predicted variations of 3% for the  $A_0$  mode and 10% for the  $S_0$  mode. Apart from small measurement inaccuracies, the angular dependency of the phase slowness matched the theoretical curve well for the  $A_0$  mode. For the  $S_0$  mode, a small, but consistent offset between measurements and theory was found in the non-principal directions, while good agreement was observed in the principal directions ( $\varphi = 0^\circ, 45^\circ, 90^\circ$ ). This is possibly due to the observed significant wave skew for the  $S_0$  mode wave propagation, leading to low amplitudes in the far field measurement line at the center of the angle beam transducer.

## GUIDED WAVE BEAM SKEW

3D Finite Element (FE) simulations, described in more detail in [18], were conducted using ABAQUS Explicit to visualize the guided wave field amplitude and beam skew. The guided wave field in the area in front of the wedge transducer was measured with 21 steps of 1 mm perpendicular to the excitation line at the center of the angle beam transducer and 9 steps of 5 mm along the investigated crystallographic direction, covering an area of 20 mm by 40 mm. Figure 5 shows the measured and predicted  $A_0$  mode guided wave fields for different orientations of the silicon wafer relative to the angle beam transducer and monitoring grid. For all directions, a clear and strong guided wave beam can be observed from the measurements. A slight widening of the beam is observed for directions with lower stiffness <100> compared to the <110> direction (with the highest stiffness). The measured wave field in the principal crystallographic direction is not perfectly symmetric due to experimental inaccuracies, but wave propagation along the symmetry line (dots) can be observed for the <110> and <100> directions. Beam skew with a small angle can be seen in the non-principal directions ( $\varphi = 15^\circ, 30^\circ$ ) with the maximum amplitude off-center in the far-field. Similar behavior can be observed in the FE simulation results, with the guided wave fields perfectly symmetric for the  $0^\circ$  and  $45^\circ$  directions, and small beam skew for the  $15^\circ$  and  $30^\circ$  directions.

For the  $S_0$  mode shown in Fig. 6, again reasonably good agreement between measurements and FE simulations was obtained. For the high stiffness crystallographic direction <110> a strong guided wave beam was measured, with a small deviation from the symmetry line. Significantly larger beam skew than for the  $A_0$  mode was observed in the non-principal directions ( $\varphi = 15^\circ, 30^\circ$ ). Significant widening of the guided wave beam can be seen for directions with lower stiffness compared to the <110> direction and to the  $A_0$  mode wave fields. For the <100> principal direction with the lowest stiffness, the guided wave amplitude drops quite rapidly with distance from the wedge transducer and a very wide area with similar amplitudes can be observed. This is well predicted by the FE simulations, which show a significant beam skew in the non-principal directions and symmetric wave fields for the principal directions. Some differences in the predicted beam skew and widening can be observed in Fig. 6 compared to the experimental measurements. The beam skew angle of the measured and simulated wave fields was evaluated and compared to theoretical predictions using Disperse [19]. The theoretical wave skew angle was extracted from the phase slowness curves and is shown in Fig. 7 for the  $A_0$  and  $S_0$  mode. It should be noted that the configuration assumed in theory is different from the experimental and FE geometries, where the width of the transducer and excitation line relative to the wavelength are not small (approximately  $6\lambda$  for the  $A_0$  mode,  $3\lambda$  for the  $S_0$  mode). For each perpendicular line, the amplitude values were interpolated to a step size of 0.1 mm to achieve better accuracy. The location of the maximum amplitude value and the relative 3 dB and 6 dB drops on both sides of the pulse were obtained. The angle of the beam skew was obtained for the maxima and the centers of the 3dB and 6dB amplitude drop lines.

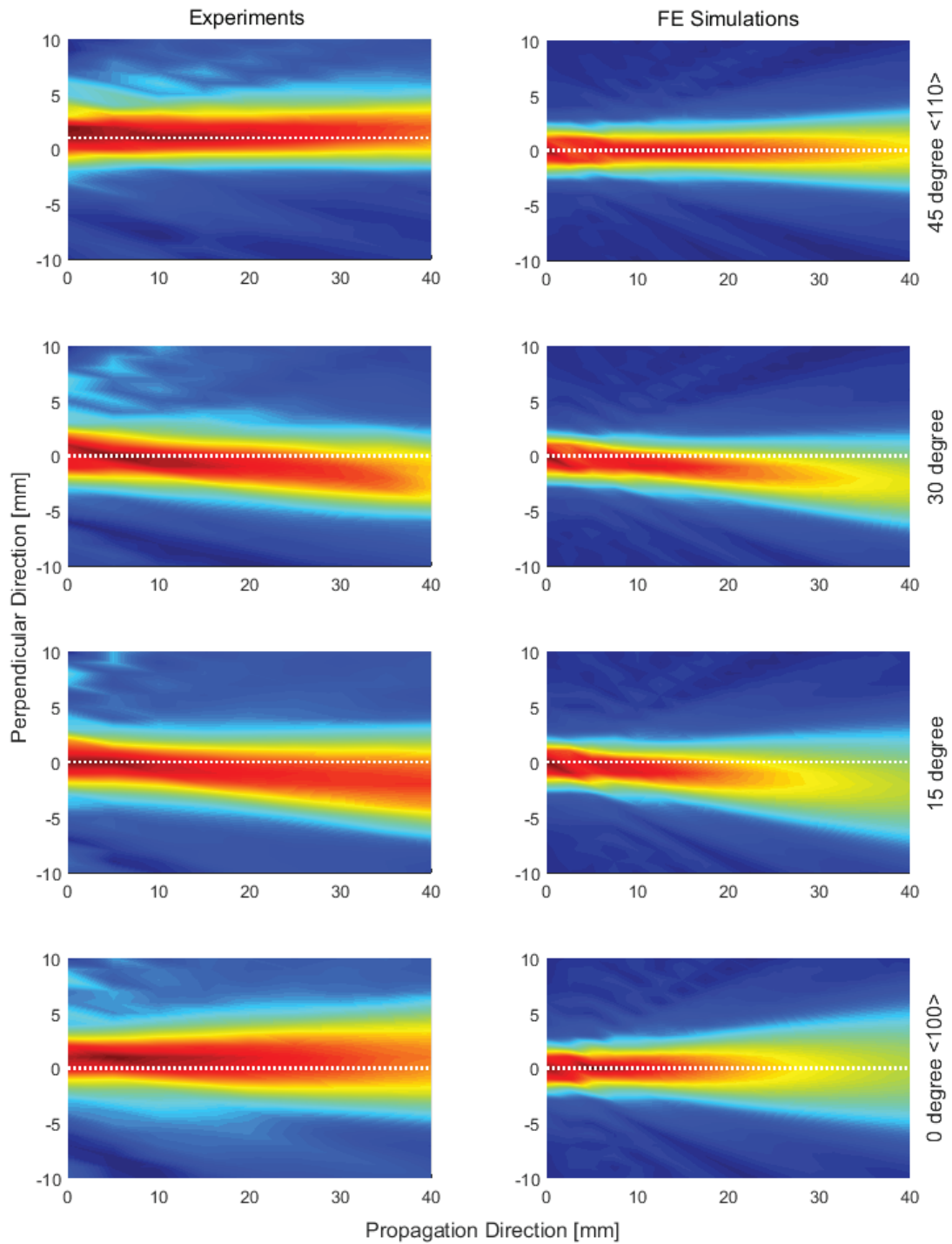


**FIGURE 5.** Experimental measurement (left) and FE simulation (right) of guided wave beam skew; evaluation of amplitude (FFT) at each monitoring location for  $A_0$  mode, excitation along different crystallographic orientations:  $\varphi = 0^\circ$  ( $\langle 100 \rangle$  crystal orientation),  $\varphi = 15^\circ$ ,  $\varphi = 30^\circ$ ,  $\varphi = 45^\circ$  ( $\langle 110 \rangle$  crystal orientation).

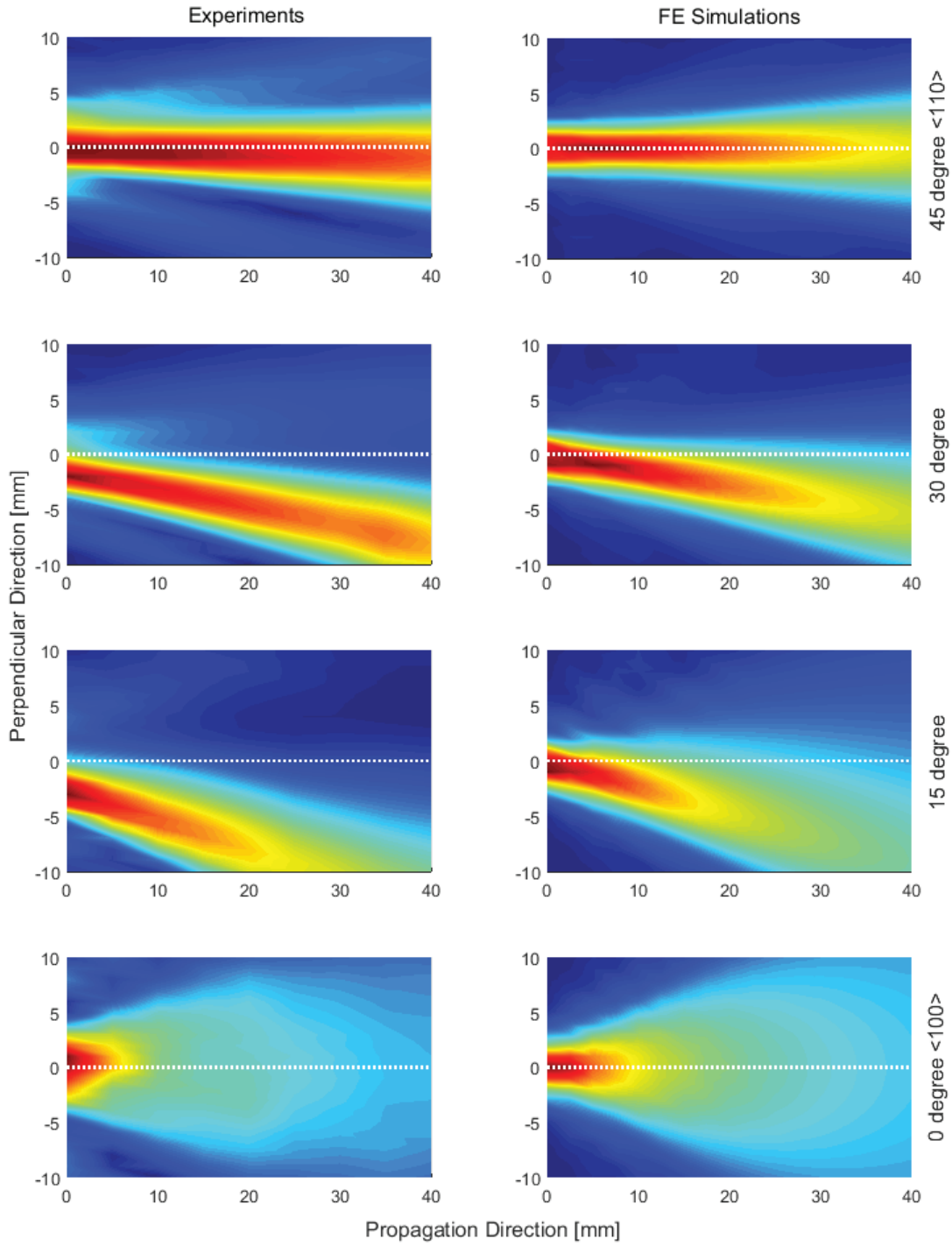


**FIGURE 6.** Experimental measurement (left) and FE simulation (right) of guided wave beam skew; evaluation of amplitude (FFT) at each monitoring location for  $S_0$  mode, excitation along different crystallographic orientations:  $\varphi = 0^\circ$  ( $\langle 100 \rangle$  crystal orientation),  $\varphi = 15^\circ$ ,  $\varphi = 30^\circ$ ,  $\varphi = 45^\circ$  ( $\langle 110 \rangle$  crystal orientation).

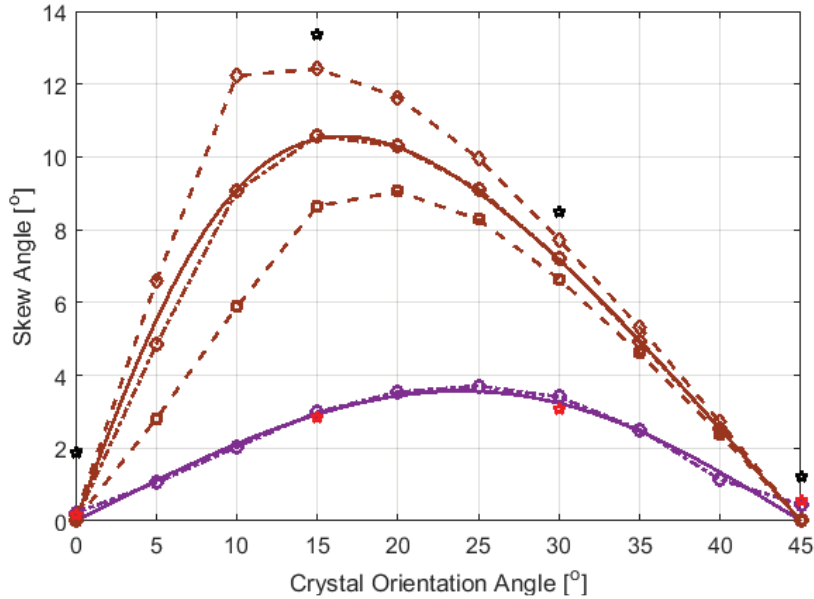


**FIGURE 7.** Wave skew angles for  $A_0$  (purple solid lines, red dots) and  $S_0$  (brown solid lines, black dots) modes: theory (solid), experiments 3dB drop centers (stars); FE evaluation: maximum (diamonds, dashed), 3dB drop centers (circles, dash-dotted), 6 dB drop centers (squares, dashed).

For the  $A_0$  mode the theoretically predicted maximum skew angle is  $3.6^\circ$ , as can be seen in Fig. 7. Good agreement of the FE simulations with theory can be observed, irrespective of the evaluation method (maximum value, 3 dB amplitude drop, 6 dB amplitude drop). For the  $A_0$  mode, a strong wave pulse with symmetry to the skew direction was observed in Fig. 5, in good approximation, the excitation can be assumed similar to a line source with a width of approximately  $6\lambda$ . The experimentally observed skew angles for propagation directions of  $15^\circ$  and  $30^\circ$  relative to the  $\langle 100 \rangle$  crystal orientation show good agreement with theoretical calculations. For the principal directions, the difference between measured and predicted skew angles is at most  $0.3^\circ$ , this difference is possibly due to misalignment of the wafer and transducer. Theoretical calculations predict a larger maximum skew angle of  $10.6^\circ$  for the  $S_0$  mode, in line with the observed larger variation of the phase slowness. For the FE simulations in propagation directions at an angle to the  $\langle 110 \rangle$  direction, a significant beam widening and asymmetry of the beam relative to the maximum amplitude on each perpendicular line can be seen (Fig. 6). Depending on the evaluation methodology, an over-estimation of the beam skew angle (line of maximal amplitude) or under-estimation (center line of 6 dB drop) is observed in Fig. 7. The center line for a 3 dB amplitude drop appears to match the theoretical predictions, but this very likely depends on the excitation width (for  $S_0$  mode approximately  $3\lambda$ ) and should not be over-interpreted. A general agreement of the observed skew angles is obtained, but exact values depend on the configuration and evaluation method. Experimental values are shown using the 3 dB drop evaluation. Skew angles of up to  $1.9^\circ$  were observed for the  $S_0$  mode in the principal directions, a larger error than observed for the  $A_0$  mode. The experimentally observed beam skew in the non-principal directions is consistently larger than predicted from theory and observed for the FE simulations (see Fig. 6). More research will be required to ascertain whether this corresponds to measurement inaccuracies or whether some of the assumptions are not valid for the experimental setup.

## CONCLUSIONS

Guided wave propagation in single crystal silicon wafers was measured experimentally and simulated using 3D FE models. The material anisotropy results in a dependency of the wave propagation characteristics on the direction relative to the crystallographic orientation. Measured phase velocities for the fundamental  $A_0$  and  $S_0$  modes in general match well with the theoretically predicted phase slowness curves. The larger variation of the  $S_0$  phase slowness by about 10% leads to significant skew angles of up to  $11^\circ$  for the guided wave beam. Similar beam skew and widening behavior was observed for both fundamental modes between experimental measurements and FE simulations. For the  $A_0$  mode, variations in the phase slowness of about 3% for different propagation directions lead to beam skew angles below  $4^\circ$ , with good agreement to theoretical predictions. For the  $S_0$  mode, asymmetries and an influence of the skew angle evaluation method were observed. For this mode, systematically larger skew angles have been measured when compared to the FE simulations and predicted from theory.

## REFERENCES

1. A. Luque and S. Hegedus, *Handbook of Photovoltaic Science and Engineering*, Wiley, New York (2011).
2. M. Abdelhamid, R. Singh and M. Omar, *IEEE J. Photovoltaics* **4**, 514-524 (2014).
3. M. Israil, A. Ghani and Y. Kerm, *Phys. Sci. Int. J.* **4**, 1073-1087 (2014).
4. J. L. Rose, *Mat. Eval.* **60**, 53-59 (2002).
5. P. Fromme, "Health Monitoring of Plate Structures using Guided Waves," *Proc. SPIE* **6935**, 69350W (2008).
6. B. Masserey and P. Fromme, *Insight* **51**, 667-671 (2009).
7. B. Masserey and P. Fromme, *NDT&E Int.* **71**, 1-7 (2015).
8. M.-K. Song and K.-Y. Jhang, *Advances in Materials Science and Engineering*. Vol. **2013**, 950791 (2013).
9. S. K. Chakrapani, M.J. Padiyar and K. Balasubramaniam, *J. Nondestruct. Eval.* **31**, 46-55 (2012).
10. H. J. Maris, *J. Acoust. Soc. Am.* **50**, 812-818 (1971).
11. K. Y. Kim, K.C. Bretz, A.G. Every and W. Sachse, *J. Appl. Phys.* **79**, 1857-1863 (1996).
12. B. Audoin, C. Bescond and M. Deschamps, *J. Appl. Phys.* **80**, 3760-3771 (1996).
13. C. Prada, D. Clorennec, T.W. Murray and D. Royer, *J. Acoust. Soc. Am.* **126**, 620-625 (2009).
14. M. Veidt and W. Sachse, *J. Acoust. Soc. Am.* **96**, 2318-2326 (1994).
15. B. I. S. Murat, P. Khalili and P. Fromme, *J. Acoust. Soc. Am.* **139**, 3044-3052 (2016).
16. A. Leleux, P. Micheau and M. Castaings, *J. Nondestruct. Eval.* **32**, 200-214 (2013).
17. B. Chapuis, N. Terrien and D. J. Royer, *Acoust. Soc. Am.* **127**, 198-203 (2010).
18. P. Fromme, M. Pizzolato, J.-L. Robyr and B. Masserey, *J. Acoust. Soc. Am.* **143**, 287-295 (2018).
19. B. Pavlakovic, M. J. S. Lowe, D. Alleyne and P. Cawley, "Disperse: A general purpose program for creating dispersion curves," *Rev. Prog. QNDE* **16**, (eds) D.O. Thompson and D.E. Chimenti, Plenum Press, New York, pp. 185-192 (1997).